Activation behavior for ion permeation in ion-exchange membranes: Role of ion dehydration in selective transport

Journal of Membrane Science

Revised: February 2, 2019

Razi Epsztein, Evyatar Shaulsky, Mohan Qin, and Menachem Elimelech*

Department of Chemical and Environmental Engineering, Yale University, New Haven, Connecticut 06520-8286, USA

* Corresponding author. E-mail: menachem.elimelech@yale.edu; Tel: +1 (203) 432-2789

Graphical abstract

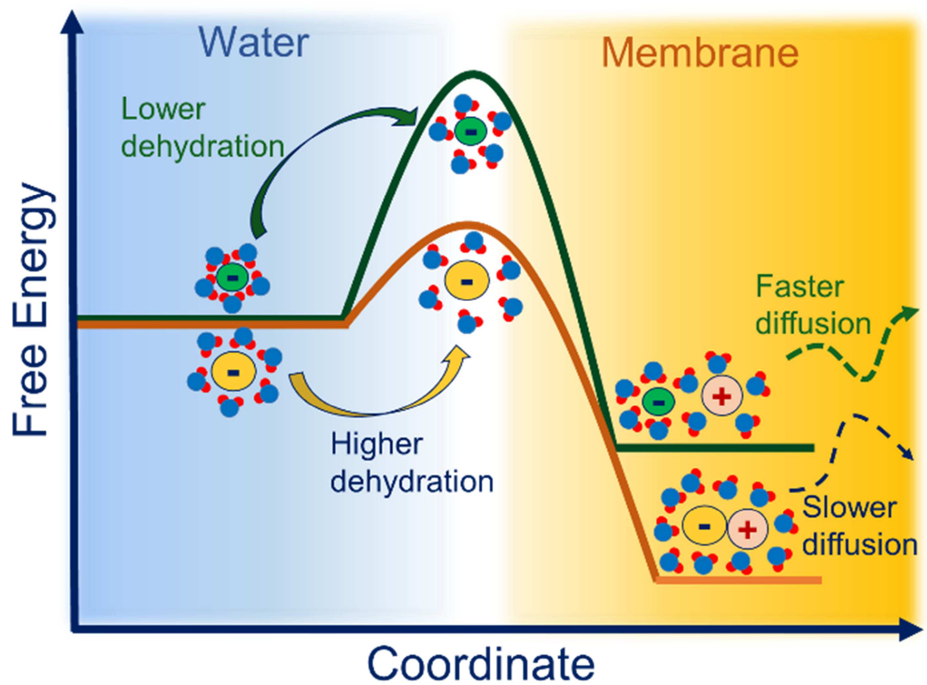

Highlights

- The mechanisms underlying the selectivity of ion-exchange membranes are explored.
- Ions show activation behavior of transport according to an Arrhenius-type equation.
- Smaller and more strongly hydrated ions show higher energy barrier for transport.
- Smaller and more strongly hydrated ions show higher pre-exponential factor.
- Activation behavior of ion transport is attributed to ion dehydration.

ABSTRACT

We explored the mechanisms governing the selectivity of anion- and cation-exchange membranes for the transport of four monovalent anions (i.e., fluoride, chloride, bromide, and nitrate) and four monovalent cations (i.e., sodium, potassium, cesium, and ammonium), respectively. Our ion adsorption and transport tests with mixed ion solutions reveal that an ion with larger ionic radius and lower hydration energy is more favorably adsorbed onto the ion-exchange membrane but diffuses more slowly through the polymer matrix compared to an ion with smaller ionic radius and higher hydration energy. Individual anion (as sodium salt) or cation (as chloride salt) permeation tests through the ion-exchange membranes at different temperatures were performed to evaluate the activation behavior of ion transport through the ion-exchange membranes by calculating the energy barrier and pre-exponential factor (i.e., the ion flux when the energy barrier is negligible) for ion transport from an Arrhenius-type equation. Our results show that an ion with smaller ionic radius and higher hydration energy experiences higher energy barrier (e.g., fluoride, 10.3 kcal mol^{-1}) and possesses higher pre-exponential factor compared to an ion with larger ionic radius and lower hydration energy (e.g., bromide, 4.6 kcal mol^{-1}). This correlation corroborates our main hypothesis that the activation behavior observed for ion transport is a result of ion dehydration at the water-membrane interface. Our proposed ion selectivity mechanism elucidates how ion dehydration governs the extent of ion permeation into the membrane and the subsequent transport through the charged polymer matrix. Future membrane design that promotes dehydration of target ions is challenging but can result in unprecedented ion selectivity.

Keywords: ion-exchange membrane; ion selectivity; ion dehydration; energy barrier; Arrhenius-type equation

1. Introduction

Selective removal of small target ions and low-molecular-weight contaminants from water is technologically challenging but can reduce operational costs and minimize brine disposal [1–5]. Pressure-driven (e.g., reverse osmosis and nanofiltration) and electro-driven (e.g., electrodialysis and membrane capacitive deionization) membrane technologies can address this challenge to a limited extent [6–9]. In these processes, the membrane pore selectivity for a specific solute is predominantly dictated by steric (size)- and Donnan (charge)-exclusion mechanisms, rendering the membrane relatively unselective when species with similar size or charge are present [10–14]. The extent to which an ion is rejected from the membrane by size- and charge-exclusion mechanisms is well correlated to its hydrated size and charge, respectively [15–19]. Nevertheless, consistent selectivity trends (yet minor) are observed in these membranes, even for solutes having similar hydrated size and charge, as in the commonly observed case of monovalent anions (e.g., nitrate permeates more favorably than chloride through nanofiltration and ion-exchange membranes) [20–25].

Hydration energy (i.e., the amount of energy released when one mole of ion undergoes hydration) is used to explain the selectivity of ions possessing similar hydrated size and charge [26–28]. In general, ions with higher hydration energy are more effectively rejected by reverse osmosis [29,30], nanofiltration [31,32], and ion-exchange membranes [3,26,27,33–35]. Hydration energy can also explain the order of elution of monovalent ions from ion chromatography [36–38]. Here, a monovalent ion with higher hydration energy (e.g., fluoride) is eluted from the column before a monovalent ion with lower hydration energy (e.g., bromide). However, while the effect of ion hydrated radius and charge on selectivity is attributed to the size- and charge-exclusion mechanisms, respectively, the exact mechanism relating hydration energy to the observed ion selectivity is not fully understood.

Over the last decade, extensive research using molecular dynamics simulations showed that water molecules surrounding an ion in solution (i.e., the hydration shell) can be partially removed during ion permeation through uncharged nanopores that are smaller than the hydrated size of the ion [39–42]. This partial removal of water molecules, known as ion dehydration, contributes to the overall energy barrier associated with ion transport through the pore due to the thermodynamically more favorable form of the hydrated ion compared to the non-hydrated ion.

Differences in dehydration-based energy barriers were shown to boost selectivity between ions permeating through nanopores [42–45]. In ion selective biological channels, ion dehydration plays a crucial role to obtain selectivity [46,47]. In these channels, specific binding sites for ions within the channel compensate for the energetic cost of dehydration by providing favorable compensatory interactions with the ion. Precise selectivity results when this energetic compensation is more favorable for one type of ion than for another, relative to the energy of dehydration [47]. That is, both the binding strength of water molecules to the ion before dehydration and the interaction of the dehydrated ion with its new surrounding after dehydration dictate the selectivity.

Numerous studies have shown that ions permeating through polymeric membranes show activation behavior [48–52]; that is, the ion flux is dependent exponentially on the temperature according to an Arrhenius-type equation [53–56]. The Arrhenius-type equation connects the ion flux to the energy barrier associated with the ion permeation through the membrane and a pre-exponential factor representing the maximum ion flux that can be obtained when the energy barrier is negligible. Based on insights from molecular dynamics simulations of ion permeation through nanopores, the mechanism of ion dehydration was also proposed to explain selectivity trends in nanofiltration membranes by correlating the experimental energy barrier for ion permeation to its hydration energy [20,21,48]. Specifically, Richards et al. [48] showed experimentally that the fluoride anion experiences the highest energy barrier among other monovalent anions while permeating through a pressure-driven nanofiltration membrane. The authors attributed the relatively high energy barrier of fluoride to its much higher hydration energy, corresponding to a much stronger and less easy-to-remove hydration shell compared to other anions. However, results from this work could not show correlation between experimental energy barriers and hydration energies of other anions (e.g., chloride and nitrate) [48].

In contrast to reverse osmosis and nanofiltration membranes, ion-exchange membranes are permeable to counterions but almost impermeable to co-ions and water. This exclusive transport of counterions through the membrane is due to the high thickness of the membrane and the significant amount of fixed charged groups within the polymer matrix that inhibits the permeation of co-ions and promotes adsorption of counterions [57–61]. As in biological channels [46,47], this counterion-exchange phenomenon at the solution-membrane interface is expected to energetically compensate for the loss of the hydration shell of the ion, reduce the overall energy barrier for ion permeation, and facilitate its transport along the thick polymer matrix.

Previous studies modelling ion partitioning and transport in ion-exchange membranes have accounted for the solvation state of the ion [62–68]. In particular, these studies have focused on the ion solvation free energy change that arises when the ion moves from one dielectric (i.e., water) into another (i.e., membrane polymer). However, direct experimental evaluation of the energy barrier associated with ion transport through ion-exchange membranes has not been reported. Specifically, the energetic penalty due to changes in ion solvation at the water-membrane interface has not been experimentally quantified.

The objective of this study is to experimentally explore the mechanisms governing the selectivity of ion-exchange membranes in light of the growing efforts to understand and improve ion selectivity. Our study of the permeation of four monovalent anions and four monovalent cations through anion- and cation-exchange membrane, respectively, shows that both anions and cations present activation behavior of transport. Using an Arrhenius-type equation, we found that an ion with smaller ionic radius and higher hydration energy experiences higher energy barrier and diffuses faster in the ion-exchange membrane compared to an ion with larger ionic radius and lower hydration energy. This correlation provides experimental evidence for the role of ion dehydration in activation behavior of transport and highlights the potential to increase selectivity between similar counterions based on their ability to undergo dehydration.

2. Materials and methods

2.1 Materials and chemicals

Commercial anion- and cation-exchange membranes (AMI-7001 and CMI-7000, respectively, Membrane International) were used for all ion adsorption and transport tests. Unless otherwise indicated, membranes were immersed in 1 M sodium chloride (NaCl) solution overnight before use. Sodium fluoride (NaF), sodium nitrate ($NaNO_3$), sodium sulfate (Na_2SO_4), potassium chloride (KCl), cesium chloride (CsCl), and ammonium chloride (NH_4Cl) were purchased from Sigma-Aldrich. Sodium chloride (NaCl) and magnesium chloride hexahydrate ($MgCl_2{\cdot}6H_2O$) were purchased from J.T. Baker Chemicals. Sodium bromide (NaBr) was purchased from Fisher

Science Education. Deionized water (MilliPore Academic A-10, resistance 15 MΩ-cm) was used for preparing solutions, equilibration of membranes, and rinsing the diffusion cell.

2.2 Characterization of ion-exchange membranes

The commercial AMI-7001 and CMI-7000 ion-exchange membranes were selected for this study due to their functional ion-exchange groups (i.e., quaternary ammonium and sulfonate groups, respectively) and high robustness. A thorough characterization of the membranes is essential to understand their ion transport behavior and selectivity.

Transport number of the membranes was measured using the potentiometric method [3]. Briefly, each membrane (surface area of 14.5 cm^2) was placed between two chambers containing NaCl at concentrations of 0.01 M and 0.1 M (Fig. S1). The chambers were rigorously mixed to minimize concentration polarization and allow ion diffusion from the high- to low-concentration chamber. The membrane potential (i.e., the difference in electric potential between the two sides of the membrane) established due to the selectivity of the membrane for anions or cations was continuously monitored using a voltmeter (Fluke 77 Multimeter) and recorded for 30 min after stabilization. The average membrane potential during these 30 min was used to calculate the transport number using

$$\Delta E = (2t_m - 1)\frac{RT}{nF}\ln\left(\frac{\alpha_1}{\alpha_2}\right) \quad (1)$$

where ΔE is the measured membrane potential, t_m is the transport number, R is the universal gas constant (8.314 J K^{-1} mol^{-1}), F is the Faraday constant (96485 C mol^{-1}), and α_1 and α_2 are the activities of the high- and low-concentration chambers, respectively [69].

The membrane inherent selectivity for transport of counterions, the permselectivity, accounts for both the transport number of counterions within the membrane and the transport number in the bulk solution according to [70]

$$Permselectivity = \frac{t_m - t_i}{1 - t_i} \quad (2)$$

Here, t_m is the membrane transport number as determined from Eq. (1) and t_i is the transport number of the counterion in the bulk solution (0.39 and 0.61 for Na^+ and Cl^-, respectively), derived from its relative diffusion coefficient in water [71].

The ion-exchange capacity of the membranes was determined by the exchange of previously adsorbed ions (i.e., Na^+ or Cl^-) with another ion. After immersing both membranes in 1 M NaCl solution, the anion- and cation-exchange membranes were washed thoroughly with DI water to remove excess of salt and then immersed in a 1 M solution of NaBr and KCl, respectively. Besides the high concentration used (1 M), Br^- and K^+ have higher affinity to the anion- and cation-exchange membranes compared to Cl^- and Na^+, respectively, and therefore are expected to provide an efficient exchange [3]. We used anion (Dionex DX-500 with an AS14A IonPac column) and cation (Dionex ICS-1000 with a CS14 IonPac column) chromatography to measure the anion (i.e., Cl^- and Br^-) and cation (i.e., Na^+ and K^+) concentration in the solutions, respectively, before and after the exchange.

For water uptake measurement, small pieces of dry anion- and cation-exchange membranes were weighted as supplied (i.e., without immersing in NaCl solution) and then immersed in DI water for 24 hr. After 24 hr, the membranes were wiped gently and weighted again. The water uptake was calculated as the percentage (wt.%) of water accumulated in the membrane.

Membrane thickness was measured using cross section images of the membrane taken with scanning electron microscopy (SEM, Hitachi SU-70). Before imaging, membrane samples were sputter-coated with a chromium layer (BTT-IV, Denton Vacuum, LLC, Moorestown, NJ).

We also verified the functional groups on the surface of the anion- and cation-exchange membranes (quaternary ammonium and sulfonate groups, respectively). Dry membrane samples were tested as supplied with attenuated total reflectance Fourier transform infrared (ATR FTIR) spectroscopy (Thermo Nicolet 6700 FT-IR Spectrometer, Thermo Fisher Scientific Inc.) to identify typical bonds and stretches associated with the quaternary amine headgroups and sulfonates. Energy-dispersive X-ray analysis (EDX) with SEM was used to detect the specific elements characterizing the functional groups (i.e., nitrogen and sulfur) and adsorbed counterions (i.e., chloride and sodium) on the membrane surface.

2.3 Ion adsorption onto ion-exchange membranes

The extent of adsorption of each ion onto the anion- and cation-exchange membranes was measured using mixed solutions containing four anions (i.e., F^-, Cl^-, Br^-, and NO_3^- as sodium salts) or four cations (i.e., Na^+, K^+, Cs^+, and NH_4^+ as chloride salts), respectively, at a concentration of 2.5 mM for each salt. Mixed solutions were used, rather than single-salt solutions, to take into account possible competition for adsorption among the ions. Before immersing the membranes in the mixed ion solutions, the anion- and cation-exchange membranes were immersed in 1 M Na_2SO_4 and 1 M $MgCl_2$ solutions, respectively, for 24 hr to exchange previously adsorbed ions with SO_4^{2-} or Mg^{2+} ions. The membranes were then washed with DI water to remove excess of Na_2SO_4 and $MgCl_2$ solution and immersed in the mixed solutions described above for additional 24 hr. Following adsorption, anion and cation concentration in the solution were analyzed using anion and cation chromatography, respectively. Sulfate and magnesium ions, which are not part of the ions investigated in our study, were used to ensure a proper comparison by exchanging previously adsorbed ions (the membranes are supplied with Cl^- and Na^+ as counterions). The experiment was performed at a temperature of 25°C. Adsorption was calculated as percentage of decrease in the solution anion or cation concentration.

2.4 Selectivity of ion-exchange membranes

The selectivity of anion- and cation-exchange membranes for the transport of specific anion or cation, respectively, was measured in a custom-made diffusion cell (Fig. S2). A mixed anion (i.e., F^-, Cl^-, Br^-, and NO_3^- as sodium salts) or cation (i.e., Na^+, K^+, Cs^+, and NH_4^+ as chloride salts) solution at a concentration of 0.1 M for each salt was placed in the side chambers (the mixed anion and cation solutions were used in separate experiments) and was separated from the middle chamber by the anion- and cation-exchange membranes (each with surface area of 14.5 cm^2). The middle chamber was filled with DI water and mixed with a stir bar. The two side chambers were continuously mixed together to maintain electroneutrality. Before each experiment, the anion- and cation-exchange membranes were immersed overnight in the same mixed anion or cation solution of the specific experiment to exchange previously adsorbed ions.

During the selectivity experiments, ions diffused from the side chambers to the middle chamber through the anion- and cation-exchange membranes due to the concentration gradient. A conductivity meter (Oakton, Con 2700) was placed in the middle chamber to monitor the increase in conductivity over time. When conductivity in the middle chamber reached 1000 µS

cm^{-1}, samples were taken from the middle cell and analyzed by anion or cation chromatography. Reaching this stage (i.e., conductivity of 1000 µS cm^{-1} in the middle chamber) lasted several hours, ensuring that ion transport was stable. Moreover, the ion concentrations in the middle chamber at this stage could be reliably detected by anion and cation chromatography. The selectivity of X^- anion (i.e., F^-, Cl^-, Br^-, and NO_3^-) over Cl^- anion, $P_{Cl^-}^{X^-}$, and the selectivity of X^+ cation (i.e., Na^+, K^+, Cs^+, and NH_4^+) over Na^+ cation, $P_{Na^+}^{X^+}$, were calculated using

$$P_{Cl^-}^{X^-} = \frac{J_{X^-}/J_{Cl^-}}{C_{X^-}/C_{Cl^-}} \tag{3}$$

$$P_{Na^+}^{X^+} = \frac{J_{X^+}/J_{Na^+}}{C_{X^+}/C_{Na^+}} \tag{4}$$

where J_i is the flux of component i through the membrane and C_i is the average concentration of component i in the side (concentrated) chambers. Because of the much higher volume of the solution in the side chambers (0.3 L) compared to the middle chamber (35 mL), the concentration of ions in the side chambers almost did not change over time and remained ~ 0.1 M. Therefore, the denominator in Eqs. (3) and (4) was assumed to be 1. The flux of each ion was calculated by dividing its amount in the middle chamber at the final stage (i.e., 1000 µS cm^{-1} in the middle chamber) by the time elapsed to reach the final stage and the surface area of the membrane. The selectivity experiments were performed at a temperature of 25°C.

2.5 Determination of energy barrier and pre-exponential factor for ion transport

Experimental energy barriers (*Ea*) and pre-exponential factors (*A*) for anion (i.e., F^-, Cl^-, Br^-, and NO_3^- as sodium salts) and cation (i.e., Na^+, K^+, Cs^+, and NH_4^+ as chloride salts) transport through the anion- and cation-exchange membranes, respectively, were determined from an Arrhenius-type equation using single-salt solutions (initial concentration of 0.25 M):

$$J = A\exp\left(-\frac{E_a}{RT}\right) \tag{5}$$

where J is the ion flux through the membrane, R is the universal gas constant, and T is the absolute temperature.

The single-salt solution was placed in the side chambers and the middle chamber was filled with DI water (Fig. S2). The same mixing regime of the middle and side chambers was applied as in the selectivity measurement. Before each experiment, the anion- and cation-exchange membranes were immersed overnight in the same single-salt solution of the specific experiment to exchange previously adsorbed ions. During the experiment, ions diffused from the side chambers to the middle chamber through the anion- and cation-exchange membranes due to the concentration gradient. A conductivity meter was placed in the middle chamber to monitor the increase in electric conductivity over time.

For this set of experiments, the diffusion cell was placed in a temperature-controlled bath with a heater. Temperature was increased in 5°C increments every 100 min, from 25°C to 40°C, and monitored by both a standard thermometer that was placed in the bath and the heater itself (which was equipped with an internal thermometer). For all increments, temperature stabilized in less than 50 min, allowing a stable flux measurement afterwards (Fig. S3). Therefore, for each temperature, the average ion flux (*J*) was calculated from the slope of the increase in conductivity over time during the latter 50 min. The natural logarithm of the ion flux, ln*(J)*, was then plotted as a function of (1/*T*) and the energy barrier (*Ea*) and pre-exponential factor (*A*) were determined from the linearized form of the Arrhenius-type equation:

$$ln(J) = \ln(A) - \frac{E_a}{R}\left(\frac{1}{T}\right) \qquad (6)$$

3. Results and discussion

3.1 Characteristics of ion-exchange membranes

The anion- and cation-exchange membranes (AMI-7001 and CMI-7000, respectively) are dense, nonporous polymer films. According to the manufacturer, the membranes are made of a polystyrene backbone cross-linked with divinylbenzene and chemically functionalized with ion-exchange groups, namely, quaternary ammonium and sulfonic acid for the anion- and cation-exchange membranes, respectively. We verified the functional groups on the surface of the anion- and cation-exchange membrane using ATR FTIR spectroscopy (Fig. S4). Two distinctive peaks detected at absorbance of 956 cm^{-1} and 1039 cm^{-1} are associated with the quaternary amine headgroup (N-C, red) and the symmetric stretch of sulfonate group (S=O, blue), respectively [72]. SEM-EDX elemental mapping confirmed the presence of nitrogen and chlorine originating from the quaternary ammonium groups and chloride counterions, respectively, on the surface of the anion-exchange membrane (Fig. S5). Sulfur and sodium, originating from the sulfonic acid groups and sodium counterions, respectively, were detected on the surface of the cation-exchange membrane (Fig. S6).

The main properties measured for the ion-exchange membranes are summarized in Table 1. The calculated transport number for both anion- and cation-exchange membranes indicated non-ideal behavior of co-ion exclusion [73] but was higher than 0.9, confirming the dominant presence of counterions in the membranes due to the Donnan-exclusion effect [74]. A lower permselectivity value was calculated for the anion- than for the cation-exchange membrane as reported previously [58]. While the reason for such difference can be related to the higher ion-exchange capacity of the cation-exchange membrane [58], we also surmise that the sulfonate functional groups, with smaller size (and therefore higher charge density) and more polar structure, are more effective in electrostatically excluding co-ions compared to quaternary ammonium functional groups.

Table 1

The ion-exchange capacity of both the anion- and cation-exchange membrane (per unit volume) is much greater than the capacity of ionized carboxyl groups of a typical polyamide RO (SW30) membrane [75], explaining the high permselectivity of the ion-exchange membranes for counterions and suggesting that electrostatic adsorption at the water-membrane interface might play a major role in ion transport and selectivity. We measured the membrane thickness using a cross-section SEM image (Fig. S7). Although water flux through the ion-exchange membranes is negligible due to their high thickness (and therefore high hydraulic resistance), water content of both anion- and cation-exchange membranes was approximately 20% due to hydration of the ionic groups within the membrane and other hydrophilic portions of the polymer matrix [57].

3.2 Order of ion adsorption onto ion-exchange membranes

We explored the selectivity of the anion- and cation-exchange membrane for the transport of four monovalent anions (i.e., F^-, Cl^-, Br^-, and NO_3^-) and four monovalent cations (i.e., Na^+, K^+, Cs^+, and NH_4^+), respectively. Important properties of these anions and cations (i.e., ionic radius and hydration energy) that govern their transport behavior in ion-exchange membranes are summarized in Tables 2 and 3, respectively. According to the solution-diffusion model, ion transport through a dense nonporous membrane can be divided into two distinctive steps: adsorption (i.e., partitioning) onto the polymer matrix and diffusion through the membrane [60]. Therefore, we evaluated first the adsorption of the four anions (Fig. 1a) and four cations (Fig. 2a) onto the anion- and cation-exchange membrane, respectively, to identify adsorption-induced selectivity trends. To support our proposed mechanism for the adsorption order of the ions, we compared the adsorption trends obtained for the ion-exchange membranes to the adsorption behavior of the anions and cations in anion (Fig. 1b) and cation (Fig. 2b) chromatography.

Table 2

Table 3

Figure 1

Figure 2

For anions (Fig. 1), the order of adsorption onto the anion-exchange membrane (NO_3^- > Br^- > Cl^- > F^-) correlates to the reverse order of the hydration energy of the anions (Table 2). That is, an anion with higher hydration energy showed lower adsorption onto the membrane after 24 hr compared to an anion with lower hydration energy. Similar results were obtained after three hours of adsorption (Fig. S8), suggesting that at 24 hr, equilibrium state was reached and the rate of adsorption did not play a role in the results observed. This set of results obtained at equilibrium indicate that an anion with higher hydration energy (e.g., F^-) has lower affinity to the membrane polymer matrix and its adsorption is less favorable thermodynamically compared to an anion with lower hydration energy (e.g., NO_3^-). We attribute the lower affinity of an anion with higher hydration energy to the polymer matrix to its less easy-to-remove hydration shell which interrupts with the formation of strong electrostatic bonds with the positively charged quaternary ammonium functional groups in the membrane compared to an anion with lower hydration energy. In general, the easier it is to remove the hydration shell of an ion, the higher the dehydration an ion can undergo. Ion dehydration can also explain the order of anion elution from anion chromatography (Fig. 1b). Here, an anion with lower hydration energy that can remove more easily water molecules from its hydration shell (e.g., NO_3^-) develops stronger electrostatic bonds with the fixed quaternary ammonium groups in the resin which result in longer residence time in the column during elution compared to an anion with higher hydration energy (e.g., F^-) [36].

Similar trends were observed for the three spherical monoatomic cations (Na^+, K^+, and Cs^+) tested (Fig. 2). A cation with higher hydration energy (e.g., Na^+) showed lower adsorption onto the cation-exchange membrane at equilibrium and was eluted earlier from the cation chromatography compared to a cation with lower hydration energy (e.g., Cs^+), generalizing the proposed mechanism of ion dehydration for both anions and cations. Ammonium (NH_4^+), with slightly lower hydration energy than K^+, was less adsorbed onto the cation-exchange membrane and eluted earlier from the column compared to K^+. We attribute this deviation to the polyatomic tetrahedral structure of NH_4^+ which might interfere with its binding to the negative sulfonate groups in the membrane or the carboxylate groups in the chromatography resin compared to the spherical monoatomic cations (discussed later in Section 3.6). The similarity between adsorption trends in ion-exchange membranes and ion chromatography for both anions and cations suggests that ion properties (e.g., the hydration energy), rather than specific adsorbent properties (e.g. structure and type of functional groups), govern the adsorption order in the investigated ion-exchange systems and therefore supports the mechanism of ion dehydration.

3.3 Selectivity order of ion-exchange membranes

Membrane selectivity for a specific ion accounts for both ion adsorption (i.e., partitioning) onto the ion-exchange membrane and ion diffusion within the membrane [3]. We measured the transport rate of the four anions and four cations through the anion- and cation-exchange membranes, respectively, in mixed salt solutions containing the four anions (as sodium salts) or four cations (as chloride salts). We then calculated the selectivity of each anion (Fig. 3a) or cation (Fig. 3b) over Cl^- or Na^+, respectively, according to Eqs. (3) and (4), respectively.

Figure 3

For anions (Fig. 3a), the selectivity order ($Br^- > NO_3^- > Cl^- > F^-$) was the same as the adsorption order ($NO_3^- > Br^- > Cl^- > F^-$), except for the swap between Br^- and NO_3^- in the series (i.e., NO_3^- was better adsorbed than Br^- but the membrane was more selective to Br^- than to NO_3^-). This selectivity order, including the higher transport of Br^- than NO_3^-, was reported previously for some anion-exchange membranes [76,77]. For cations (Fig. 3b), except for the location of Na^+ in the series compared to the other cations, the selectivity order ($NH_4^+ > K^+ \sim Cs^+ > Na^+$) was different than the adsorption order ($Cs^+ > K^+ > NH_4^+ > Na^+$) and, in general, showed minor differences between the monoatomic cations. While the selectivity of specific cation-exchange membranes for all the four cations in the series was not investigated in the literature, the higher selectivity for K^+ over Na^+ was reported in a few studies [3,78].

Generally, for both anions and cations our results indicate that ion diffusion within the membrane (i.e., the second stage of ion transport based on the solution-diffusion model) mitigated the effect of adsorption (i.e., the first stage of ion transport) on the overall selectivity, resulting in differences between selectivity and adsorption trends. These results suggest that more favorably adsorbed ions with higher affinity to the polymer matrix have lower diffusion within the membrane (e.g., Cs^+ was more favorably adsorbed than K^+ but diffused more slowly through the membrane). In general, an ion with higher affinity to the membrane develops stronger attraction bonds with the fixed groups in the polymer matrix that inhibit its diffusion within the membrane compared to an ion with lower affinity to the membrane. This proposed mechanism is supported by the elution order of the ions from ion chromatography (Fig. 1b and Fig. 2b), showing that an ion with lower affinity to the resin (e.g., F^-) is eluted faster from the resin than an ion with higher affinity (e.g., NO_3^-).

3.4 Activation behavior of ion transport through ion-exchange membranes

Activation behavior of ion transport can be evaluated by relating ion flux to temperature according to an Arrhenius-type equation (Eq. (5)) [48–52]. From this relationship, the energy barrier and pre-exponential factor (i.e., the ion flux when the energy barrier is negligible) for ion transport can be calculated. In contrast to measurement of ion flux solely, calculation of energy barriers and pre-exponential factors also accounts for the temperature and therefore can provide mechanistic insights into ion transport that flux measurement, by itself, cannot. The energy barrier experienced by the ion can result from different mechanisms hindering its transport through the membrane (e.g., charge repulsion and friction with the polymer matrix). Ion dehydration during the transport of ions from bulk solution into a confined environment is another mechanism that was demonstrated to contribute to the overall energy barrier for ion permeation through nanopores [40,41] and nanofiltration membranes [21,48].

To better explain the mechanisms of ion permeation through the membranes and the resulted selectivity, we measured individually the flux of each anion (as sodium salt) and each cation (as chloride salt) through the anion- and cation-exchange membrane (Fig. 4 and Fig. 5, respectively) at four different temperatures to obtain the energy barrier (Ea) and the pre-exponential factor (A) from the linearized form of the Arrhenius-type equation (Eq. (6)). Specifically, we first measured the increase in ion conductivity in the middle chamber at four different temperatures due to ion diffusion from the side chambers (Fig. 4a and Fig. 5a). We then calculated the ion flux for each temperature (50 min segments) and plotted the natural logarithm of the flux, $\ln(J)$, as a function of $1/T$ (Fig. 4b and Fig. 5b). To improve the clarity of the presented results, for each point in Fig. 4b and Fig. 5b the flux was normalized to the flux at 25°C.

Figure 4

Figure 5

Generally, all the ions investigated in this study showed an activation behavior with linear dependence between $\ln(J)$ and $1/T$ ($R^2 > 0.99$). We attribute this highly temperature-correlated activation behavior to the diffusion-only transport of ions through the membrane (i.e., ion transport was driven only by concentration gradient). For both monoatomic anions (Fig. 6a) and monoatomic cations (Fig. 6b), the calculated energy barriers correlated to the hydration energies of the ions, suggesting that an ion with higher hydration energy needs to overcome a higher energy barrier while permeating through the membrane.

Figure 6

This correlation between energy barriers and hydration energies links the hydration energy, an inherent ion property, to the energy barrier associated with ion permeation through the ion-exchange membrane. More specifically, it implies that the strength of ion hydration plays an important role in ion transport through the polymer matrix and supports the previously proposed mechanism of ion dehydration [41,48]: an ion with higher hydration energy (and therefore stronger hydration shell) undergoes lower dehydration compared to an ion with lower hydration energy. Importantly, our calculated energy barriers in relatively thick ion-exchange membranes are comparable to previously determined energy barriers for monovalent anions in nanopores and nanofiltration membranes with much thinner active layer [41,42,48], suggesting that the barriers arise mainly at the pore (or polymer matrix) entrance as discussed previously [42,43]. The fact that these energy barriers arise at the polymer entrance further supports the proposed mechanism of ion dehydration at the water-membrane interface.

Notably, the pre-exponential factor *A* (i.e., the inherent maximum ion flux through the membrane when the energy barrier for transport is negligible) calculated for the monoatomic anions (Fig. 6a) and monoatomic cations (Fig. 6b) also correlated to the hydration energy of the ions. This correlation supports our results for ion selectivity in the previous section, suggesting that an ion with stronger hydration shell and lower affinity to the polymer matrix (e.g., F^-) diffuses faster through the ion-exchange membrane compared to an ion with weaker hydration shell and higher affinity to the polymer matrix (e.g., Br^-). As discussed above, the faster diffusion of an ion with lower affinity to the polymer matrix compared to the diffusion of an ion with higher affinity to the polymer matrix can also explain the elution order of ions from ion chromatography.

To support the trend observed for the energy barrier and pre-exponential factor in Fig. 6, we repeated the experiments for individual solutions of NaF, NaCl, and KCl three more times each using a new set of anion- and cation-exchange membranes (Fig. S9). As in Fig. 6, our measured energy barriers and pre-exponential factors for different ions were significantly different from each other and correlated to ion hydration energy ($F^- > Cl^-$; $Na^+ > K^+$).

3.5 Mechanisms of ion transport through ion-exchange membranes

We showed for both anions and cations that at equilibrium the adsorption of ions with lower hydration energy onto the ion-exchange membrane is thermodynamically more favorable compared to the adsorption of ions with higher hydration energy (Fig. 1a and Fig. 2a). Therefore, an ion with larger ionic radius and lower hydration energy reaches a lower (and therefore more favorable) free energy state after adsorption onto the membrane compared to an ion with smaller ionic radius and higher hydration energy (Fig. 7a). We also demonstrated that monovalent ions show activation behavior of transport through the membrane where, for monoatomic ions, an ion with larger ionic radius and lower hydration energy experiences lower energy barrier of permeation through the ion-exchange membrane compared to an ion with smaller ionic radius and higher hydration energy (Fig. 7a). As discussed above, this cumulatively calculated energy barrier for ion transport through the membrane arises mainly at the water-membrane interface due to the transition of ions from bulk solution into the confined environment of the membrane polymer.

Figure 7

We attribute these differences in the energy barrier and Gibbs free energy change (ΔG) of adsorption to the different ability of each ion to partially remove water molecules from its hydration shell during permeation through the ion-exchange membrane, as previously suggested for nanofiltration membranes [21,48]. In general, this ability of an ion to undergo partial dehydration depends on both the strength of its hydration shell (expressed as the hydration energy) and the interaction between the dehydrated ion with its new surrounding after dehydration, as proposed for ion-selective biological channels [46,47]. However, in ion-exchange membranes, without perfect matching sites as in biological channels, the extent of dehydration undergone by an ion is primarily dictated by the strength of its hydration shell. That is, an ion with higher hydration energy (e.g., F^-) undergoes lower dehydration than an ion with lower hydration energy (e.g., Br^-).

Due to its higher dehydration, an ion with lower hydration energy can approach closer to the fixed charged functional groups in the membrane and develop stronger electrostatic interactions with the fixed groups, resulting in more favorable adsorption and higher affinity to the polymer matrix compared to an ion with higher hydration energy. This distance-dependent electrostatic attraction between the mobile counterions and the fixed ions in the membrane can be described by Coulomb's law [79]. A similar mechanism was proposed to explain the selectivity order in ion chromatography where an ion with higher hydration energy (e.g., F^-) develops weaker interactions with the fixed charged groups on the resin and therefore is eluted from the chromatography column earlier compared to an ion with lower hydration energy (e.g., Br^-) [36].

Because of its higher dehydration-based energy barrier, an ion with smaller ionic radius and higher hydration energy will statistically occupy less fixed charged sites on the membrane surface during its transport in the membrane compared to an ion with larger ionic radius and lower hydration energy (Fig. 7b). However, due to the lower affinity of an ion with higher hydration energy to the polymer matrix, it is less hindered and can diffuse faster through the membrane as supported by its higher pre-exponential factor *A* (Fig. 6) compared to an ion with lower hydration energy (Fig. 7b). Overall, our proposed mechanism suggests that adsorption at the water-membrane interface, rather than diffusion within the polymer matrix, is the key step for the observed selectivity in ion-exchange membranes.

3.6 Why energy barriers of nitrate and ammonium do not follow the trend with hydration energy?

The energy barriers calculated for the polyatomic ions (i.e., NO_3^- and NH_4^+) were slightly higher considering their hydration energies, resulting in discrepancy between the trends of hydration energies and calculated energy barriers. Specifically, NO_3^- has the lowest hydration energy among the anions but showed a higher energy barrier than Br^-; similarly, NH_4^+, with slightly lower hydration energy than K^+, experienced higher energy barrier than K^+. We attribute this behavior of NO_3^- and NH_4^- to geometrical and orientation effects that may impose an additional energy barrier for their transport (Fig. 8).

Unlike spherical monoatomic anions such as Cl^- (Fig. 8a), NO_3^-, with a trigonal planar molecular geometry [80], may need to be in a specific orientation in order to enter the membrane pore (Fig. 8b). This orientation adjustment is on top of other energy-consuming barriers at the water-membrane interface (e.g., overcome charge repulsion and undergo dehydration) and therefore contributes to the overall energy barrier of permeation. Previously calculated energy barriers for anion permeation in nanofiltration membrane also showed a discrepancy with ion hydration energies, where NO_3^- anion experienced higher energy barrier for permeation than other anions with higher hydration energies such as Cl^- or Br^- [20,21,48].

Ammonium is made up of four equally spaced sp^3 hybrid orbitals forming a tetrahedral geometry with bond angles of 109.5° [80]. Although this geometry provides NH_4^+ with a symmetrical 3D structure (i.e., a rotation around any axis results in a molecule indistinguishable from the original), differences in electron densities around the molecule may render some areas on the surface (i.e., the vertices) sterically less approachable than others (i.e., the faces).

Therefore, it is likely that in a specific orientation, the distance between the center of the NH_4^+ cation and the center of the fixed negatively charged group in the membrane can be minimized due to reduced steric hindrance, resulting in a thermodynamically more favorable ionic interaction (Fig. 8c). As in the case of NO_3^-, this orientation adjustment of NH_4^+ results in additional energy penalty for permeation. This hypothesis is supported by our results from cation chromatography, where the K^+ cation showed better adsorption than NH_4^+ despite having higher hydration energy. In the cation chromatography, NH_4^+ developed weaker electrostatic interactions with the functional negatively charged groups in the resin and was eluted before K^+, presumably due to steric limitations to form a closer (and therefore more stable) ionic interaction.

4. Conclusion

We explored the mechanisms underlying the selectivity of anion- and cation-exchange membranes for the transport of four monovalent anions (i.e., fluoride, chloride, bromide, and nitrate) and four monovalent cations (i.e., sodium, potassium, cesium, and ammonium), respectively. We first verified the previously reported order of ion adsorption and selectivity in the membranes where, in general, an ion with lower hydration energy is more favorably adsorbed but more slowly transported compared to an ion with higher hydration energy. Our individual ion permeation tests through the ion-exchange membranes at different temperatures showed activation behavior of ion transport through the ion-exchange membranes for all the ions investigated; namely, the ion flux depends exponentially on the temperature according to an Arrhenius-type equation. For spherical ions, both the energy barrier and the pre-exponential factor (that where derived from the Arrhenius-type equation) correlated to ion hydration energy, relating the activation behavior of ion transport to the phenomenon of ion dehydration and supporting the theory of ion dehydration-related selective transport. In particular, our calculated experimental energy barrier are comparable with previously reported energy barriers for nanofiltration membranes with much thinner active layer. This observation highlights the major contribution of ion dehydration at the water-membrane interface to the overall energy barrier and invites future studies to explore chemical functionalization of membranes that can promote ion dehydration in a more selective manner.

Acknowledgements

This research was supported by CENT, an Energy Frontier Research Center funded by the U.S. Department of Energy, Office of Science, Basic Energy Sciences under Award No. DE-SC0019112, and by a postdoctoral fellowship (to R. E.) provided by the United States-Israel Binational Agricultural Research and Development (BARD) Fund, Fellowship number FI-549-2016. Facilities used were supported by the Yale Institute of Nanoscale and Quantum Engineering (YINQE) and Chemical and Biophysical Instrument Center (CBIC). Sample analyses with ion chromatography were conducted at the Yale Analytical and Stable Isotope Center at Yale's Institute for Biospheric Studies with the help of Jonas Karosas. We also acknowledge Akshay Deshmukh from the Department of Chemical and Environmental Engineering at Yale University for valuable discussions.

Appendix A. Supplementary material

Supplementary data associated with this article can be found in the online version.

References

[1] J.R. Werber, A. Deshmukh, M. Elimelech, The Critical Need for Increased Selectivity, Not Increased Water Permeability, for Desalination Membranes, Environ. Sci. Technol. Lett. 3 (2016) 112–120. doi:10.1021/acs.estlett.6b00050.

[2] J.R. Werber, C.O. Osuji, M. Elimelech, Materials for next-generation desalination and water purification membranes, Nat. Rev. Mater. 1 (2016) 1–15. doi:10.1038/natrevmats.2016.18.

[3] T. Luo, S. Abdu, M. Wessling, Selectivity of ion exchange membranes: A review, J. Memb. Sci. 555 (2018) 429–454. doi:10.1016/j.memsci.2018.03.051.

[4] M.A. Shannon, P.W. Bohn, M. Elimelech, J.G. Georgiadis, B.J. Marinas, A.M. Mayes, Science and technology for water purification in the coming decades, Nature. 452 (2008) 301–310. doi:10.1038/nature06599.

[5] M. Xie, H.K. Shon, S.R. Gray, M. Elimelech, Membrane-based processes for wastewater nutrient recovery: Technology, challenges, and future direction, Water Res. 89 (2016)

210–221. doi:10.1016/j.watres.2015.11.045.

[6] A. Campione, L. Gurreri, M. Ciofalo, G. Micale, A. Tamburini, A. Cipollina, Electrodialysis for water desalination: A critical assessment of recent developments on process fundamentals, models and applications, Desalination. 434 (2018) 121–160. doi:10.1016/j.desal.2017.12.044.

[7] S. Porada, R. Zhao, A. Van Der Wal, V. Presser, P.M. Biesheuvel, Review on the science and technology of water desalination by capacitive deionization, Prog. Mater. Sci. 58 (2013) 1388–1442. doi:10.1016/j.pmatsci.2013.03.005.

[8] A.W. Mohammad, Y.H. Teow, W.L. Ang, Y.T. Chung, D.L. Oatley-Radcliffe, N. Hilal, Nanofiltration membranes review: Recent advances and future prospects, Desalination. 356 (2015) 226–254. doi:10.1016/j.desal.2014.10.043.

[9] L. Shan, Y. Liang, L. Prozorovska, G.K. Jennings, S. Ji, S. Lin, Multifold Enhancement of Loose Nanofiltration Membrane Performance by Intercalation of Surfactant Assemblies, Environ. Sci. Technol. Lett. 5 (2018) 668–674. doi:10.1021/acs.estlett.8b00430.

[10] J. Luo, Y. Wan, Effects of pH and salt on nanofiltration-a critical review, J. Membr. Sci. 438 (2013) 18–28. doi:10.1016/j.memsci.2013.03.029.

[11] B. Van Der Bruggen, A. Koninckx, C. Vandecasteele, Separation of monovalent and divalent ions from aqueous solution by electrodialysis and nanofiltration, Water Res. 38 (2004) 1347–1353. doi:10.1016/j.watres.2003.11.008.

[12] W.M. Deen, Hindered transport of large molecules in liquid-filled pores, AIChE J. 33 (1987) 1409–1425. doi:10.1002/aic.690330902.

[13] A.E. Yaroshchuk, Non-steric mechanism of nanofiltration: Superposition of donnan and dielectric exclusion, Sep. Purif. Technol. 22–23 (2001) 143–158. doi:10.1016/S1383-5866(00)00159-3.

[14] Z. Wang, Z. Wang, S. Lin, H. Jin, S. Gao, Y. Zhu, J. Jin, Nanoparticle-templated nanofiltration membranes for ultrahigh performance desalination, Nat. Commun. 9 (2018). doi:10.1038/s41467-018-04467-3.

[15] B. Tansel, Significance of thermodynamic and physical characteristics on permeation of

ions during membrane separation: Hydrated radius, hydration free energy and viscous effects, Sep. Purif. Technol. 86 (2012) 119–126. doi:10.1016/j.seppur.2011.10.033.

[16] L.D. Nghiem, A.I. Schäfer, M. Elimelech, Role of electrostatic interactions in the retention of pharmaceutically active contaminants by a loose nanofiltration membrane, J. Memb. Sci. 286 (2006) 52–59. doi:10.1016/j.memsci.2006.09.011.

[17] A. Seidel, J.J. Waypa, M. Elimelech, Role of Charge (Donnan) Exclusion in Removal of Arsenic from Water by a Negatively Charged Porous Nanofiltration Membrane, Environ. Eng. Sci. 18 (2001) 105–113. doi:10.1089/10928750151132311.

[18] W. Cheng, C. Liu, T. Tong, R. Epsztein, M. Sun, R. Verduzco, J. Ma, M. Elimelech, Selective removal of divalent cations by polyelectrolyte multilayer nanofiltration membrane: Role of polyelectrolyte charge, ion size, and ionic strength, J. Memb. Sci. 559 (2018) 98–106. doi:10.1016/j.memsci.2018.04.052.

[19] N. Dizge, R. Epsztein, W. Cheng, C.J. Porter, M. Elimelech, Biocatalytic and salt selective multilayer polyelectrolyte nanofiltration membrane, J. Memb. Sci. 549 (2018) 357–365. doi:10.1016/j.memsci.2017.12.026.

[20] R. Epsztein, W. Cheng, E. Shaulsky, N. Dizge, M. Elimelech, Elucidating the mechanisms underlying the difference between chloride and nitrate rejection in nanofiltration, J. Memb. Sci. 548 (2017) 694–701. doi:https://doi.org/10.1016/j.memsci.2017.10.049.

[21] R. Epsztein, E. Shaulsky, N. Dizge, D.M. Warsinger, M. Elimelech, Role of ionic charge density in Donnan exclusion of monovalent anions by nanofiltration, Environ. Sci. Technol. 52 (2018) 4108–4116.

[22] R. Epsztein, O. Nir, O. Lahav, M. Green, Selective nitrate removal from groundwater using a hybrid nanofiltration–reverse osmosis filtration scheme, Chem. Eng. J. 279 (2015) 372–378. doi:10.1016/j.cej.2015.05.010.

[23] F. Garcia, D. Ciceron, A. Saboni, S. Alexandrova, Nitrate ions elimination from drinking water by nanofiltration: Membrane choice, Sep. Purif. Technol. 52 (2006) 196–200.

[24] P. Mukherjee, A.K. Sengupta, Ion exchange selectivity as a surrogate indicator of relative permeability of ions in reverse osmosis processes, Environ. Sci. Technol. 37 (2003) 1432–1440. doi:10.1021/es0207495.

[25] A. Eyal, O. Kedem, Nitrate-selective anion-exchange membranes, J. Memb. Sci. 38 (1988) 101–111. doi:10.1016/S0376-7388(00)80873-X.

[26] T. Sata, T. Yamaguchi, K. Matsusaki, Effect of hydrophobicity of ion exchange groups of anion exchange membranes on permselectivity between two anions, J. Phys. Chem. 99 (1995) 12875–12882. doi:10.1021/j100034a028.

[27] T. Sata, Studies on anion exchange membranes having permselectivity for specific anions in electrodialysis - Effect of hydrophilicity of anion exchange membranes on permselectivity of anions, J. Memb. Sci. 167 (2000) 1–31. doi:10.1016/S0376-7388(99)00277-X.

[28] B. Tansel, J. Sager, T. Rector, J. Garland, R.F. Strayer, L. Levine, M. Roberts, M. Hummerick, J. Bauer, Significance of hydrated radius and hydration shells on ionic permeability during nanofiltration in dead end and cross flow modes, Sep. Purif. Technol. 51 (2006) 40–47. doi:10.1016/j.seppur.2005.12.020.

[29] L. Li, J. Dong, T.M. Nenoff, Transport of water and alkali metal ions through MFI zeolite membranes during reverse osmosis, Sep. Purif. Technol. 53 (2007) 42–48. doi:10.1016/j.seppur.2006.06.012.

[30] S.M.S. Ghiu, R.P. Carnahan, M. Barger, Mass transfer in RO TFC membranes - dependence on the salt physical and thermodynamic parameters, Desalination. 157 (2003) 385–393.

[31] L. Paugam, C.K. Diawara, J.P. Schlumpf, P. Jaouen, F. Quéméneur, Transfer of monovalent anions and nitrates especially through nanofiltration membranes in brackish water conditions, Sep. Purif. Technol. 40 (2004) 237–242. doi:10.1016/j.seppur.2004.02.012.

[32] L. Paugam, S. Taha, G. Dorange, P. Jaouen, F. Quéméneur, Mechanism of nitrate ions transfer in nanofiltration depending on pressure, pH, concentration and medium composition, J. Memb. Sci. 231 (2004) 37–46. doi:10.1016/j.memsci.2003.11.003.

[33] S. Abdu, M.C. Martí-Calatayud, J.E. Wong, M. García-Gabaldón, M. Wessling, Layer-by-layer modification of cation exchange membranes controls ion selectivity and water splitting, ACS Appl. Mater. Interfaces. 6 (2014) 1843–1854. doi:10.1021/am4048317.

[34] A. Montes-Rojas, J.A.Q. Rentería, N.B.J. Chávez, J.G. Ávila-Rodríguez, B.Y. Soto, Influence of anion hydration status on selective properties of a commercial anion exchange membrane electrochemically impregnated with polyaniline deposits, RSC Adv. 7 (2017) 25208–25219. doi:10.1039/c7ra03331a.

[35] V. V. Kotov, O. V. Peregonchaya, V.F. Selemenev, Electrodialysis of binary electrolyte mixtures with membranes modified by organic species, Russ. J. Electrochem. 38 (2002) 927–929. doi:10.1023/A:1016834300357.

[36] J.S. Fritz, Factors affecting selectivity in ion chromatography, J. Chromatogr. A. 1085 (2005) 8–17. doi:10.1016/j.chroma.2004.12.087.

[37] R.E. Barron, J.S. Fritz, Effect of functional group structure on the selectivity of low capacity anion exchangers for monovalent anions, J. Chromatogr. 284 (1984) 13–25.

[38] R.E. Barron, J.S. Fritz, Effect of functional group structure and exchange capacity on the selectivity of anion exchangers for divalent anions, J. Chromatogr. A. 316 (1984) 201–210. doi:10.1016/S0021-9673(00)96152-1.

[39] S. Sahu, M. Zwolak, Ionic selectivity and filtration from fragmented dehydration in multilayer graphene nanopores, Nanoscale. 9 (2017) 11424–11428. doi:10.1039/C7NR03838K.

[40] S. Sahu, M. Di Ventra, M. Zwolak, Dehydration as a Universal Mechanism for Ion Selectivity in Graphene and Other Atomically Thin Pores, Nano Lett. 17 (2017) 4719–4724. doi:10.1021/acs.nanolett.7b01399.

[41] L.A. Richards, A.I. Schäfer, B.S. Richards, B. Corry, The importance of dehydration in determining ion transport in narrow pores, Small. 8 (2012) 1701–1709. doi:10.1002/smll.201102056.

[42] L.A. Richards, A.I. Schäfer, B.S. Richards, B. Corry, Quantifying barriers to monovalent anion transport in narrow non-polar pores, Phys. Chem. Chem. Phys. 14 (2012) 11633–11638. doi:10.1039/c2cp41641g.

[43] B. Corry, Designing carbon nanotube membranes for efficient water desalination, J. Phys. Chem. B. 112 (2008) 1427–1434. doi:10.1021/jp709845u.

[44] C. Song, B. Corry, Intrinsic ion selectivity of narrow hydrophobic pores, J. Phys. Chem. B. 113 (2009) 7642–7649. doi:10.1021/jp810102u.

[45] J. Abraham, K.S. Vasu, C.D. Williams, K. Gopinadhan, Y. Su, C.T. Cherian, J. Dix, E. Prestat, S.J. Haigh, I. V. Grigorieva, P. Carbone, A.K. Geim, R.R. Nair, Tunable sieving of ions using graphene oxide membranes, Nat. Nanotechnol. 12 (2017) 546–550. doi:10.1038/nnano.2017.21.

[46] D.A. Doyle, J.M. Cabral, R.A. Pfuetzner, A. Kuo, J.M. Gulbis, S.L. Cohen, B.T. Chait, R. MacKinnon, The Structure of the Potassium Channel: Molecular Basis of K+ Conduction and Selectivity, Science (80-.). 280 (1998) 69–77. doi:10.1126/science.280.5360.69.

[47] E. Gouaux, R. MacKinnon, Principles of Selective Ion Transport in Channels and Pumps, Science (80-.). 310 (2005) 1461–1465. doi:10.1126/science.1113666.

[48] L.A. Richards, B.S. Richards, B. Corry, A.I. Schäfer, Experimental energy barriers to anions transporting through nanofiltration membranes, Environ. Sci. Technol. 47 (2013) 1968–1976.

[49] T. Badessa, V. Shaposhnik, The electrodialysis of electrolyte solutions of multi-charged cations, J. Memb. Sci. 498 (2016) 86–93. doi:10.1016/j.memsci.2015.09.017.

[50] V. Freger, E. Korin, J. Wisniak, E. Korngold, M. Ise, K.D. Kreuer, Diffusion of water and ethanol in ion-exchange membranes: Limits of the geometric approach, J. Memb. Sci. 160 (1999) 213–224. doi:10.1016/S0376-7388(99)00084-8.

[51] V. Freger, T.C. Arnot, J.A. Howell, Separation of concentrated organic/inorganic salt mixtures by nanofiltration, J. Memb. Sci. 178 (2000) 185–193. doi:10.1016/S0376-7388(00)00516-0.

[52] J.-Y. Chen, H. Nomura, W. Pusch, Temperature dependence of membrane transport parameters in hyperfiltration, Desalination. 46 (1983) 437–446. doi:DOI: 10.1016/0011-9164(83)87187-2.

[53] M.J. Polissar, The relation between the two constants of the Arrhenius equation, J. Am. Chem. Soc. 54 (1932) 3105–3111. doi:10.1021/ja01347a011.

[54] C.N. Hinshelwood, The present position of theory of reaction velocity, Trans. Faraday Soc.

34 (1937) 105–112.

[55] R.A. Fairclough, C.N. Hinshelwood, The functional relation between the constants of the Arrhenius equation, J. Chem. Soc., Faraday Trans.ournal Chem. Soc. (1933) 538–546.

[56] S.A. Arrhenius, Über die Reaktionsgeschwindigkeit bei der Inversion von Rohrzucker durch Säuren, Z. Phys. Chem. 4 (1889) 226–248.

[57] A.B. Yaroslavtsev, V. V. Nikonenko, Ion-exchange membrane materials: Properties, modification, and practical application, Nanotechnologies Russ. 4 (2009) 137–159. doi:10.1134/S199507800903001X.

[58] H. Jaroszek, P. Dydo, Ion-exchange membranes in chemical synthesis-a review, Open Chem. 14 (2016) 1–19. doi:10.1515/chem-2016-0002.

[59] T. Xu, Ion exchange membranes: State of their development and perspective, J. Memb. Sci. 263 (2005) 1–29. doi:10.1016/j.memsci.2005.05.002.

[60] G.M. Geise, D.R. Paul, B.D. Freeman, Fundamental water and salt transport properties of polymeric materials, Prog. Polym. Sci. 39 (2014) 1–24. doi:10.1016/j.progpolymsci.2013.07.001.

[61] A.K. Sengupta, Ion exchange in environmental processes: fundamentals, applications and sustainable technology, 1st ed., John Wiley & Sons, Inc., 2017. doi:10.1002/9781119421252.

[62] J. R. Bontha, P.N. Pintauro, Water orientation and ion solvation effects during multicomponent salt partitioning in a nafion cation exchange membrane, 49 (1994) 3835–3851.

[63] J. Palomo, P.N. Pintauro, Competitive absorption of quaternary ammonium and alkali metal cations into a Nafion cation-exchange membrane, J. Memb. Sci. 215 (2003) 103–114. doi:10.1016/S0376-7388(02)00606-3.

[64] T. Malewitz, P.N. Pintauro, D. Rear, Multicomponent absorption of anions in commercial anion-exchange membranes, J. Memb. Sci. 301 (2007) 171–179. doi:10.1016/j.memsci.2007.06.014.

[65] R. Tandon, P.N. Pintauro, Solvent effects during multicomponent ion uptake into a Nafion

cation-exchange membrane, J. Memb. Sci. 341 (2009) 21–29. doi:10.1016/j.memsci.2009.05.026.

[66] R. Tandon, P.N. Pintauro, Divalent/monovalent cation uptake selectivity in a Nafion cation-exchange membrane: Experimental and modeling studies, J. Memb. Sci. 136 (1997) 207–219. doi:10.1016/S0376-7388(97)00167-1.

[67] Y. Yang, P.N. Pintauro, Multicomponent space-charge transport model for ion-exchange membranes, AIChE J. 46 (2000) 1177–1190. doi:10.1002/aic.690460610.

[68] P.N. Pintauro, R. Tandon, L. Chao, W. Xu, R. Evilia, Equilbrium partitioning of monovalent/divalent cation-salt mixtures in Nafion cation-exchange membranes, J. Phys. Chem. 99 (1995) 12915–12924. doi:10.1021/j100034a034.

[69] A.H. Truesdell, Activity Coefficients of Aqueous Sodium Chloride from 15°C to 50°C Measured with a Glass Electrode, Science (80-.). 161 (1968) 884–886. doi:10.1126/science.161.3844.884.

[70] V.K. Shahi, S.K. Thampy, R. Rangarajan, Studies on transport properties of surfactant immobilized anion-exchange membrane, J. Memb. Sci. 158 (1999) 77–83. doi:10.1016/S0376-7388(99)00029-0.

[71] H. Farrokhzad, S. Darvishmanesh, G. Genduso, T. Van Gerven, B. Van Der Bruggen, Development of bivalent cation selective ion exchange membranes by varying molecular weight of polyaniline, Electrochim. Acta. 158 (2015) 64–72. doi:10.1016/j.electacta.2015.01.062.

[72] G. Ye, J. Lee, F. Perreault, M. Elimelech, Controlled Architecture of Dual-Functional Block Copolymer Brushes on Thin-Film Composite Membranes for Integrated “defending” and “attacking” Strategies against Biofouling, ACS Appl. Mater. Interfaces. 7 (2015) 23069–23079. doi:10.1021/acsami.5b06647.

[73] A. Daniilidis, D.A. Vermaas, R. Herber, K. Nijmeijer, Experimentally obtainable energy from mixing river water, seawater or brines with reverse electrodialysis, Renew. Energy. 64 (2014) 123–131. doi:10.1016/j.renene.2013.11.001.

[74] G.S. Adair, The theory of membrane equilibrium, Trans. Faraday Soc. 33 (1937) 1106–1116. doi:10.1039/tf9373301106.

[75] D. Chen, J.R. Werber, X. Zhao, M. Elimelech, A facile method to quantify the carboxyl group areal density in the active layer of polyamide thin-film composite membranes, J. Memb. Sci. 534 (2017) 100–108. doi:10.1016/j.memsci.2017.04.001.

[76] T. Xu, K. Hu, A simple determination of counter-ionic permselectivity in an ion exchange membrane from bi-ionic membrane potential measurements: Permselectivity of anionic species in a novel anion exchange membrane, Sep. Purif. Technol. 40 (2004) 231–236. doi:10.1016/j.seppur.2004.03.002.

[77] T. Sata, Y. Tagami, K. Matsusaki, Transport Properties of Anion-Exchange Membranes Having a Hydrophobic Layer on Their Surface in Electrodialysis, J. Phys. Chem. 102 (1998) 8473–8479. doi:10.1021/jp980380z.

[78] M. Ersöz, Diffusion and Selective Transport of Alkali Cations on Cation-Exchange Membrane, Sep. Sci. Technol. 30 (1995) 3523–3533. doi:10.1080/01496399508015133.

[79] A.A. Kaufman, B.I. Anderson, Coulomb’s Law and Stationary Electric Field, Elsevier Masson SAS, 2010. doi:10.1016/S0076-6895(10)44001-9.

[80] A.F. Wells, Structural inorganic chemistry, in: First, Oxford University Press, Oxford, 1945: pp. 397–428.

[81] Y. Marcus, Thermodynamics of Solvation of Ions, J. Chem. Soc., Faraday Trans. 89 (1993) 713–718. doi:10.1017/CBO9781107415324.004.

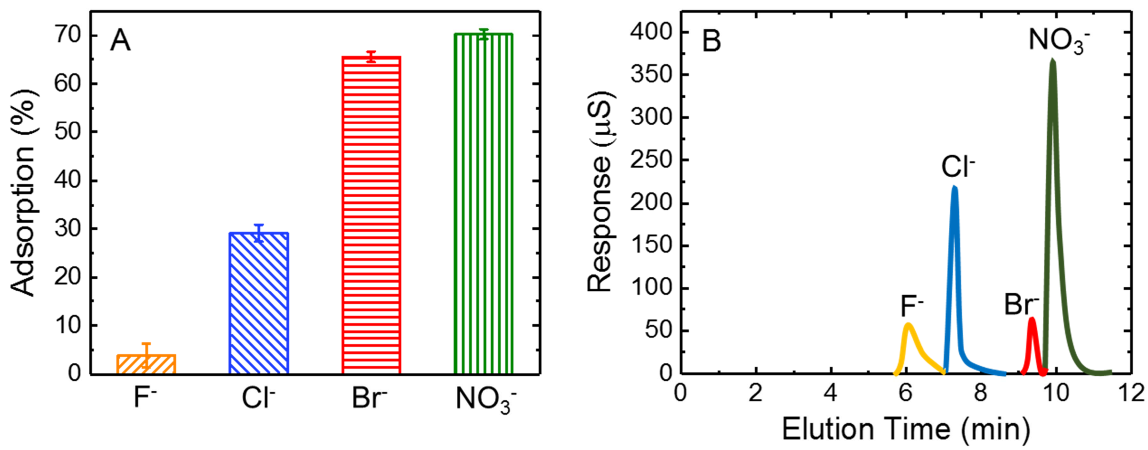

Fig 1. (A) Adsorption of fluoride (F^-), chloride (Cl^-), bromide (Br^-), and nitrate (NO_3^-) onto the anion-exchange membrane expressed as percentage of decrease in the solution anion concentration The membrane was immersed in a mixed solution containing the four anions (as sodium salts) at a concentration of 2.5 mM each. The solution was equilibrated with the membrane at 25°C and adsorption was measured after 24 h. Before the experiment, the membrane was immersed in 1 M Na_2SO_4 solution for 24 h to exchange previously adsorbed anions with SO_4^{2-}. (B) Elution order of fluoride (F^-), chloride (Cl^-), bromide (Br^-), and nitrate (NO_3^-) from anion chromatography as reflected by the anion chromatogram. A mixed anion solution containing the four anions (as sodium salts) at a concentration of 50 mg L^{-1} each (2.6 mM, 1.4 mM, 0.6 mM, and 0.8 mM for F^-, Cl^-, Br^-, and NO_3^-, respectively) was injected into the column. The column packing consisted of 9-µm diameter macroporous particles functionalized with quaternary ammonium groups. The eluent was a mixed solution of sodium carbonate (0.8 M) and sodium bicarbonate (0.1 M) solution. Peaks in the chromatogram were identified by comparing their elution times to those obtained for chromatography of single anion solution.

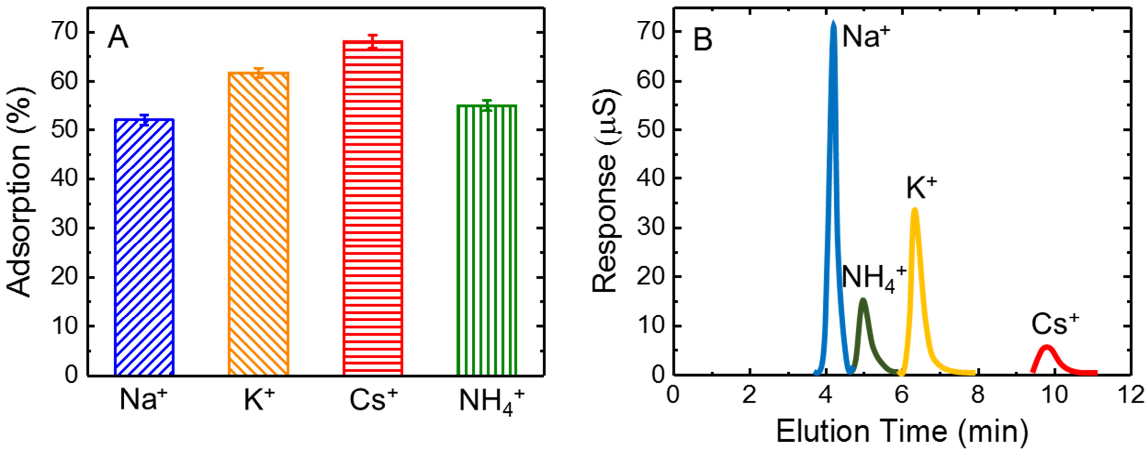

Fig 2. (A) Adsorption of sodium (Na^+), potassium (K^+), cesium (Cs^+), and ammonium (NH_4^+) onto the cation-exchange membrane expressed as percentage of decrease in the solution cation concentration. The membrane was immersed in a mixed solution containing the four cations (as chloride salts) at a concentration of 2.5 mM each. The solution was equilibrated with the membrane at 25°C and adsorption was measured after 24 h. Before the experiment, the membrane was immersed in 1 M $MgCl_2$ solution for 24 h to exchange previously adsorbed cations with Mg^{2+}. (B) Elution order of sodium (Na^+), potassium (K^+), cesium (Cs^+), and ammonium (NH_4^+) from cation chromatography as reflected by the cation chromatogram. A mixed cation solution containing the four cations (as chloride salts) in a concentration of 50 mg L^{-1} each (2.2 mM, 1.3 mM, 0.4 mM, and 2.8 mM for Na^+, K^+, Cs^+, and NH_4^+, respectively) was injected into the column. The column packing consisted of 8-µm diameter macroporous particles functionalized with carboxylate groups. The eluent was methanesulfonic acid (0.01 M) solution. Peaks in the chromatogram were identified by comparing their elution times to those obtained for chromatography of single cation solution.

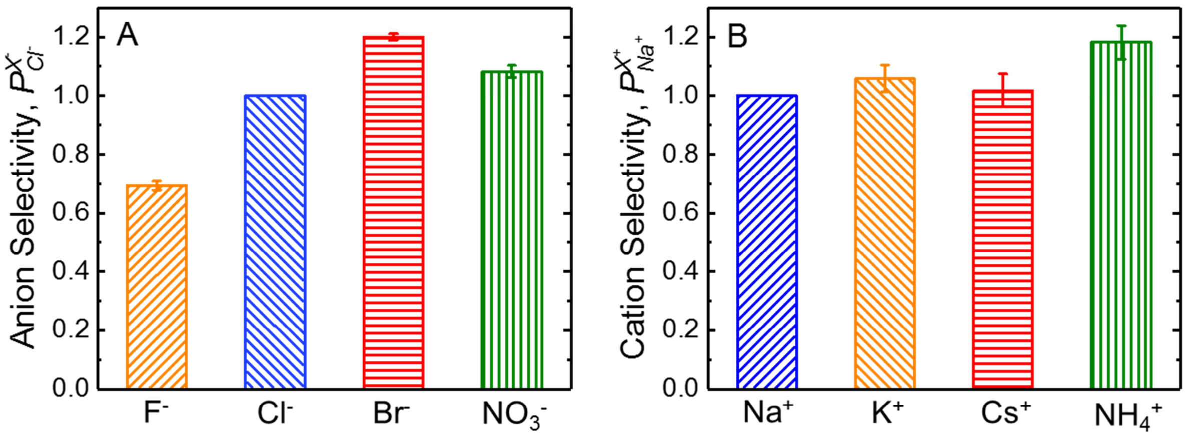

Fig 3. (A) Selectivity of X^- anion (i.e., F^-, Cl^-, Br^-, or NO_3^-) over Cl^- anion in the anion-exchange membrane. Anions diffused from the side chamber containing mixed anion solution (initial concentration of 0.1 M for each anion as sodium salt) to the middle chamber (DI water) through the anion-exchange membrane. Anion selectivity $P_{Cl^-}^{X^-}$ was calculated according to Eq. (3). (B) Selectivity of X^+ cation (i.e., Na^+, K^+, Cs^+, or NH_4^-) over Na^+ cation in the cation-exchange membrane. Cations diffused from the side chamber containing mixed cation solution (initial concentration of 0.1 M for each cation as chloride salt) to the middle chamber (DI water) through the cation-exchange membrane. Cation selectivity $P_{Na^+}^{X^+}$ was calculated according to Eq. (4). For both anions and cations, the anion- or cation-exchange membrane was equilibrated with the same mixed anion or cation solution overnight. Experiments were performed at a temperature of 25°C.

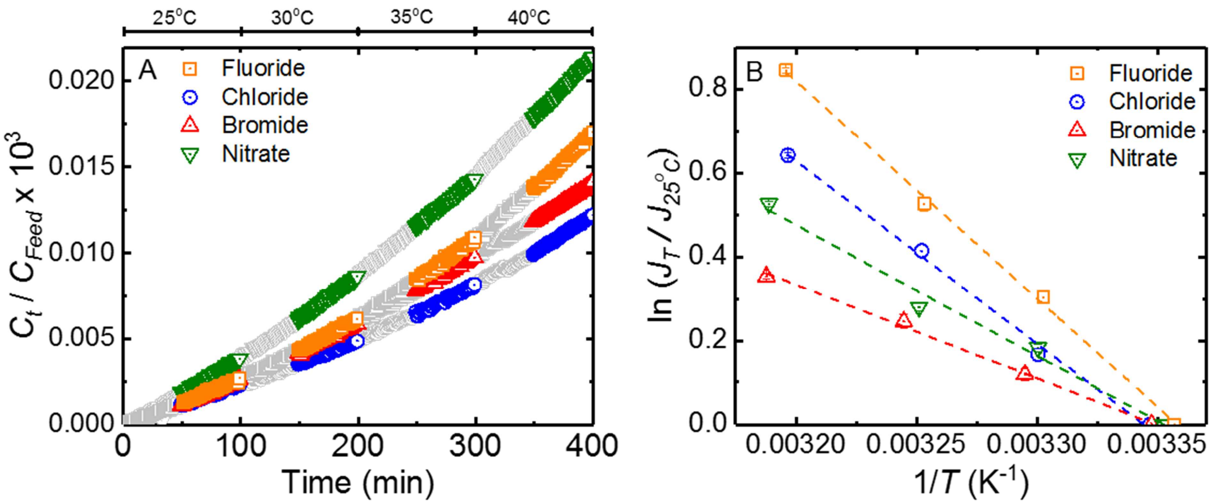

Fig 4. Activation behavior of anions (i.e., F^-, Cl^-, Br^-, and NO_3^-, as sodium salts). (A) Conductivity increase in the middle chamber as a function of time due to specific anion diffusion from the side chambers. The side chambers contained single anion solution (initial concentration of 0.25 M as sodium salt) and the middle chamber contained initially DI water (Fig. S2). Temperature was increased in 5°C increments every 100 min, from 25°C to 40°C (top axis). Since the initial conductivity of each anion in the side chambers (C_{Feed}) was different, the conductivity for each anion in the middle chamber (C_t) was normalized to the initial conductivity in the side chambers. For each temperature, the initial 50 min were given for stabilization (grey data points) and flux calculation was performed in the latter 50 min (colored data points) (B) Arrhenius-type plots for anion transport in the anion exchange membrane. For each anion, the natural logarithm of the flux (J) at the four different temperatures (normalized to the flux at 25°C) was plotted as a function of 1/T. The anion fluxes at different temperatures were calculated using linear regression of the colored data points in Fig. 4a. For each point in Fig. 4b the flux was normalized to the flux at 25°C. Error bars in Fig 4b represent standard error derived from the linear regression.

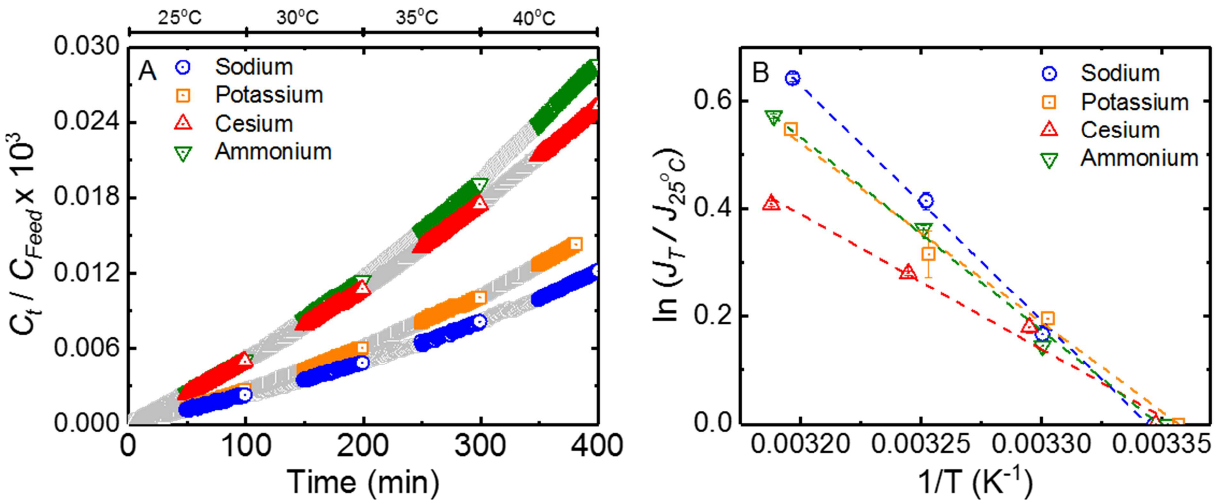

Fig 5. Activation behavior of cations (i.e., Na^+, K^+, Cs^+, and NH_4^+, as chloride salts). (A) Conductivity increase in the middle chamber as a function of time due to specific cation diffusion from the side chambers. The side chambers contained single cation solution (initial concentration of 0.25M as chloride salt) and the middle chamber contained initially DI water (Fig. S2). Temperature was increased in 5°C increments every 100 min from 25°C to 40°C (top axis). Since the initial conductivity of each cation in the side chambers (C_{Feed}) was different, the conductivity for each cation in the middle chamber (C_t) was normalized to the initial conductivity in the side chambers. For each temperature, the initial 50 min were given for stabilization (grey data points) and flux calculation was performed in the latter 50 min (data points with color) (B) Arrhenius-type plots. For each cation, the natural logarithm of the flux (J) at the four different temperatures (normalized to the flux at 25°C) was plotted as a function of 1/T. The cation fluxes at different temperature were calculated using linear regression of the colored data points in Fig. 5a. For each point in Fig. 5b the flux was normalized to the flux at 25°C. Error bars in Fig 5b represent standard error derived from the linear regression.

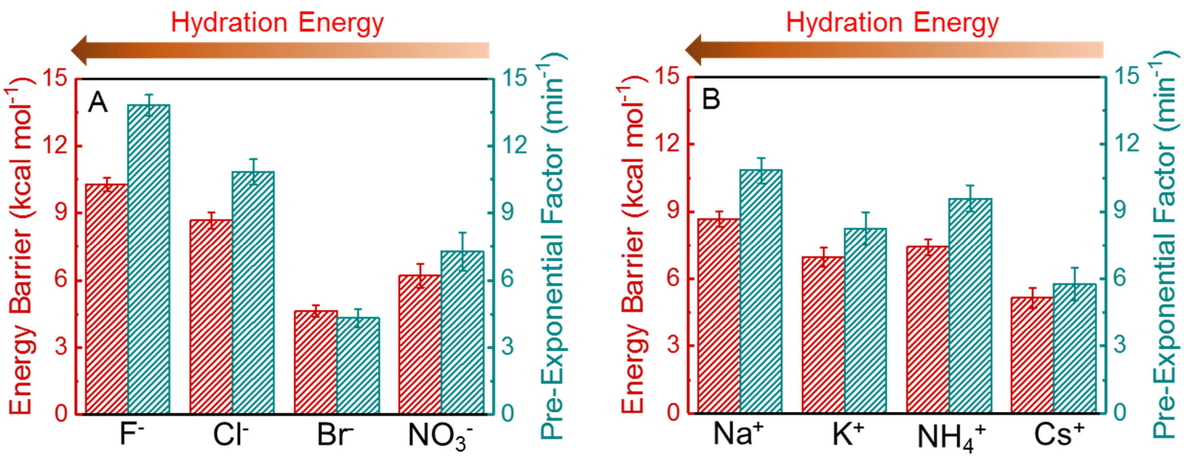

Fig 6. Experimental energy barriers and pre-exponential factors for (A) anions (i.e., F^-, Cl^-, Br^-, and NO_3^-, as sodium salts) and (B) cations (i.e., Na^+, K^+, Cs^+, and NH_4^+, as chloride salts). For each ion, the natural logarithm of the ion flux (*J*) through the membrane at four different temperatures (25°C, 30°C, 35°C, and 40°C) was plotted as a function of 1/T to obtain the energy barrier (*Ea*) and the pre-exponential factor (*A*) according to Eq. (6). The energy barrier and the pre-exponential factor were derived from linear regression of the data in Figs. 4b and 5b (before normalizing the flux to the flux at 25°C) and represent the slope and the intercept (multiplied by the membrane surface area, 14.5 cm^2) in the linear representation of the Arrhenius-type equation (Eq. (6)), respectively. All ions showed a linear dependency between ln*(J)* and *1/T* with $R^2 > 0.99$. Error bars represent standard error derived from the linear regression.

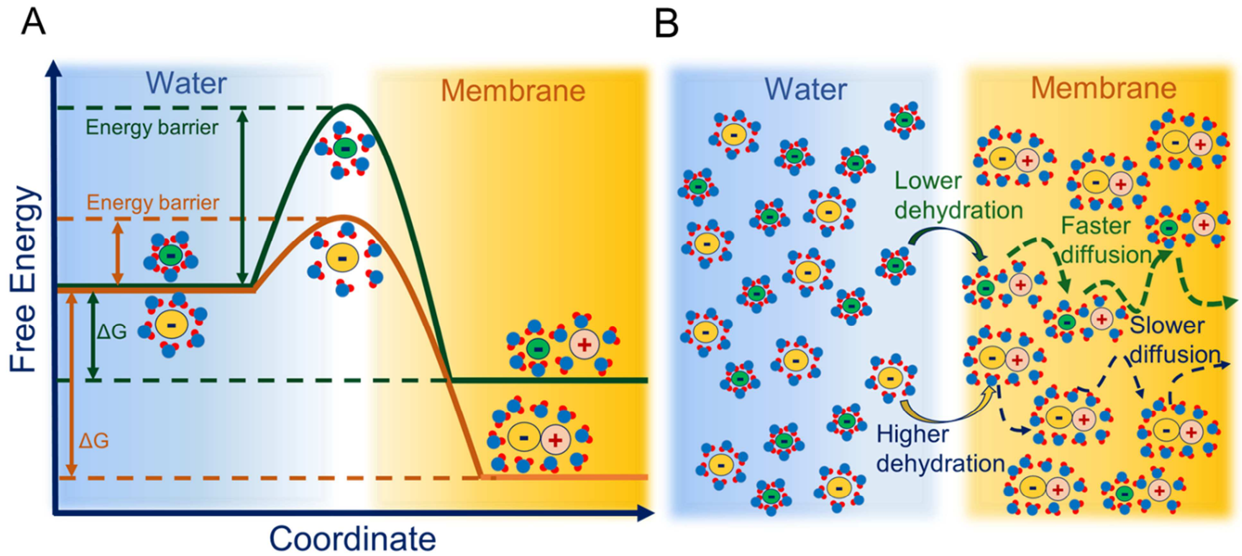

Fig 7. Proposed mechanism for the role of ion dehydration in ion transport through ion-exchange membranes illustrated by anion transport through an anion-exchange membrane. (A) Gibbs free energy change and energy barrier for anion adsorption onto an anion-exchange membrane: an anion with smaller ionic radius and stronger hydration shell (green) experiences a higher energy barrier to undergo dehydration at the water-membrane interface and reaches a higher free energy state compared to an anion with larger ionic radius and weaker hydration shell (yellow). Interaction of anions with fixed positively charged functional groups in the membrane (pink) compensate energetically for the removal of water molecules from the hydration shell of the ion and reduce the free energy state of the ion. Note that the free energy state in the membrane can be higher than the free energy state in the bulk solution, depending on the extent of chemical potential difference between the two media (B) An anion with smaller ionic radius and stronger hydration shell (green) undergoes lower dehydration and develops weaker electrostatic interactions with the fixed positively charged functional groups in the membrane (pink) compared to an anion with larger ionic radius and weaker hydration shell (yellow). Because of its higher energy barrier, an anion with smaller ionic radius occupies less fixed positively charged sites on the membrane surface compared to an anion with larger ionic radius. Due to its lower affinity to the positively charged fixed groups in the membrane, anions with smaller ionic radius are less hindered and can diffuse faster in the membrane compared to the larger anions.

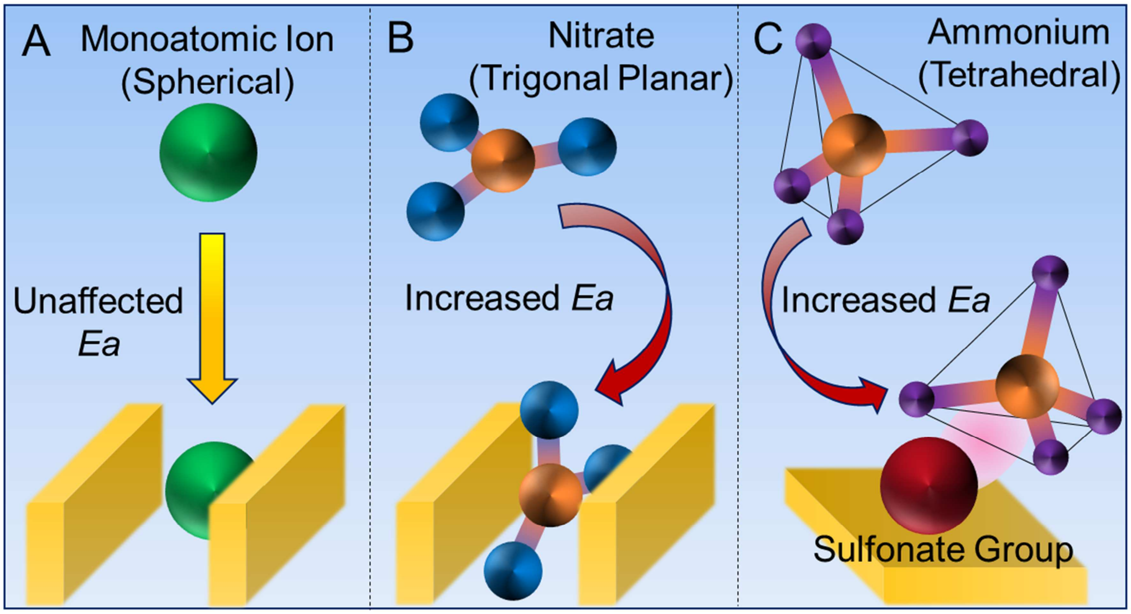

Fig 8. Proposed role of ionic geometry in ion transport. (A) Monoatomic ion (e.g., Cl^- and Na^+) represented by a green sphere: ion orientation does not play role in ion transport and does not affect the energy barrier. (B) Nitrate anion (NO_3^-) represented by a central nitrogen atom (orange sphere) surrounded by three oxygen atoms (blue spheres) in a trigonal planar geometry; orientation adjustment plays a role in ion permeation into the membrane pore and results in an increased energy barrier. (C) Ammonium cation (NH_4^+) represented by a central nitrogen atom (orange sphere) surrounded by four hydrogen atoms (purple spheres) in a tetrahedral geometry; orientation adjustment plays a role in ionic interactions with the negatively charged sulfonate group in the membrane (red sphere) and results in an increased energy barrier. All ions are illustrated without their hydration shell to emphasize shape effect on ion transport.

Table 1. Experimental characterization of the anion- and cation-exchange membranes.

Parameter	Anion-exchange membrane	Cation-exchange membrane
Transport number (t_m)	0.960 ± 0.01	0.967 ± 0.02
Permselectivity	0.900 ± 0.03	0.946 ± 0.03
Ion-exchange capacity (meq g^{-1})	1.66 ± 0.38	2.00 ± 0.21
Water uptake (wt. %)	18.3 ± 0.56	21.9 ± 0.59
Thickness (µm)	479 ± 5	490 ± 5

Table 2. Ionic radius and hydration energy of anions investigated in this study. For consistency, data was collected from the same source.[81]

Anion	Ionic radius (nm)	Hydration energy (kcal mol^{-1})
Fluoride (F^-)	0.133	111.1
Chloride (Cl^-)	0.181	81.3
Bromide (Br^-)	0.196	75.3
Nitrate (NO_3^-)	0.179	71.7

Table 3. Ionic radius and hydration energy of cations investigated in this study. For consistency, data was collected from the same source.[81]

Cation	Ionic radius (nm)	Hydration energy (kcal mol^{-1})
Sodium (Na^+)	0.102	87.2
Potassium (K^+)	0.138	70.5
Cesium (Cs^+)	0.170	59.8
Ammonium (NH_4^+)	0.148	68.1